Proceedings of ASME Turbo Expo 2011
GT2011
June 6-10, 2011, Vancouver, British Columbia, Canada

GT2011-45677

NUMERICAL INVESTIGATION OF EXHAUST DIFFUSER PERFORMANCES IN LOW PRESSURE TURBINE CASINGS

Tadashi Tanuma
Joint Program Center, Teikyo University
2-11-1, Kaga, Itabashi-ku, Tokyo 1173-8605, Japan
t-tanuma@med.teikyo-u.ac.jp

Yasuhiro Sasao Satoru Yamamoto Shinji Takada
Dept. of Computer and Mathematical Sciences, Tohoku University
Sendai 980-8579, Japan

Yoshiki Niizeki Naoki Shibukawa Hiroshi Saeki
Power and Industrial Systems Research and Development Center, Toshiba Corporation
Yokohama 230-0045, Japan

ABSTRACT

Low pressure (LP) exhaust hoods are an important component of steam turbines. The aerodynamic loss of LP exhaust hoods is almost the same as those of the stator and rotor blading in LP steam turbines. Designing high performance LP exhaust hoods should lead further enhancement of steam turbine efficiency.

This paper presents the results of exhaust hood computational fluid dynamics (CFD) analyses using last stage exit velocity distributions measured in a full-scale development steam turbine as the inlet boundary condition to improve the accuracy of the CFD analysis.

One of the main difficulties in predicting the aerodynamic performance of the exhaust hoods is the unsteady boundary layer separation of exhaust hood diffusers. A highly accurate unsteady numerical analysis is introduced in order to simulate the diffuser flows in LP exhaust hoods. Compressible Navier-Stokes equations and mathematical models for nonequilibrium condensation are solved using the high-order high-resolution finite-difference method based on the fourth-order compact MUSCL TVD scheme, Roe's approximate Riemann solver, and the LU-SGS scheme. The SST turbulence model is also solved for evaluating the eddy viscosity.

The computational results were validated using the measurement data, and the present CFD method was proven to be suitable as a useful tool for determining optimum three-dimensional designs of LP turbine exhaust diffusers.

INTRODUCTION

Power generation systems that use steam turbines produce more than half of the world's electricity. By 2035, the worldwide generation of electricity is projected to increase about 180% of the current demand [1]. Consequently, in order to supply the necessary electricity while curbing and reducing global greenhouse gas emissions, the focus should be on the development and practical realization of efficiency enhancement technologies for steam turbines used in power generation.

Figure 1 shows the cross section of a typical 1000-MW-class large-scale steam turbine and its low pressure (LP) exhaust diffusers (enveloped by four oval markers). The axial lengths and diameters of these exhaust diffusers are key factors that affect the size, weight, cost, and efficiency of the turbine system. Figure 2 gives the breakdown of the losses in a typical large-scale steam turbine such as the one shown in Figure 1. The LP exhaust hood is an important part of steam turbines. The aerodynamic loss of exhaust hoods (the third bar from the top of in Figure 2) is nearly the same as that of the stator and rotor blading (the 7th bar form the top of Figure 2) in LP steam turbines. Designing high performance LP exhaust hoods should lead further enhancement of steam turbine efficiency.

Until the first half of the 1990s, many scale tests were conducted to develop and redesign the exhaust hoods of LP turbines in order to decrease the pressure loss and increase the static pressure recovery. Since the latter half of 1990s, CFD studies have been initiated, where the goal is to optimize the aerodynamic design of the diffusers and structures in exhaust hoods. However, quantitative accuracy and sometimes even qualitative results are not sufficient to evaluate the new designs. The behavior of the inlet flow boundary layer structure, flow separations on the diffuser surface, and their unsteadiness are key reasons that result in these discrepancies [2][3].

This paper presents the numerical analyses of exhaust hood. In order to simulate the actual flow aspects more precisely, last stage exit velocity and flow angle distributions measured in the full-scale development steam turbine [4] were used as the inlet boundary conditions.

Sovran et al. [5] introduced experimentally determined optimum diffuser geometry charts that are still used by many turbomachinery manufacturers. They had already considered that the inlet flow conditions affect the optimum diffuser geometry. Xu et al. [6] showed good agreement between their numerical simulations of low pressure exhaust casings and experimental data without upstream turbine stages. Liu et al. [7-9] showed that the diffuser performance is strongly influenced by the inflow conditions. Vassiliev et al. [10] introduced CFD analysis for gas turbine exhaust diffusers with strut geometries and upstream turbine stages using the mixing plane approach. Fu et al. [11] presented a comparison between steam turbine exhaust hood tests with one-stage turbine (a stator blade row and a rotor blade row) and numerical results. Stanz et al. [12] studied the effect of tip leakage flow on an intermediate duct after the high pressure (HP) turbine stage of an aero-engine, and demonstrated that the tip leakage flow supports good pressure recovery. Fu and Liu [13] presented detailed numerical studies showing the influence of swirl angles and other inlet flow factors on the total pressure loss in a steam turbine exhaust system. These existing studies demonstrated that actual and accurate inlet flow conditions are critical when performing numerical investigations of exhaust diffusers.

One of the main difficulties in predicting the aerodynamic performance of exhaust hoods seems to be the unsteady boundary layer separations of exhaust hood diffusers. A very accurate unsteady numerical analysis [14]-[21] is introduced in order to simulate the diffuser flows in LP exhaust hoods. Compressible Navier-Stokes equations and mathematical models for nonequilibrium condensation are solved by the high-order high-resolution finite-difference method that is based on the fourth-order compact MUSCL TVD scheme, Roe's approximate Riemann solver [22], and the LU-SGS scheme [23]. The SST turbulence model is also solved for the evaluating the eddy-viscosity [24].

The computational results were validated by the measurement data and the present CFD method was proven to be suitable as a useful tool for determining optimum three-dimensional (3D) designs of LP turbine exhaust diffusers.

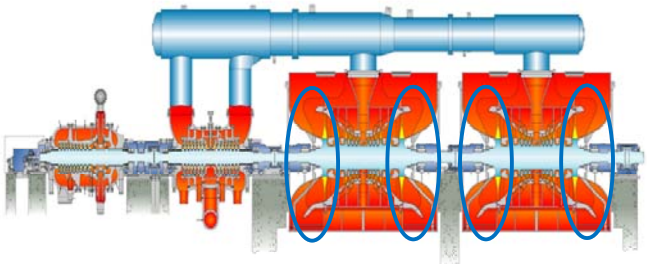

Figure 1. TYPICAL LARGE-SCALE STEAM TURBINE AND LP EXHAUST DIFFUSERS (ENVELOPED BY FOUR OVAL MARKERS)

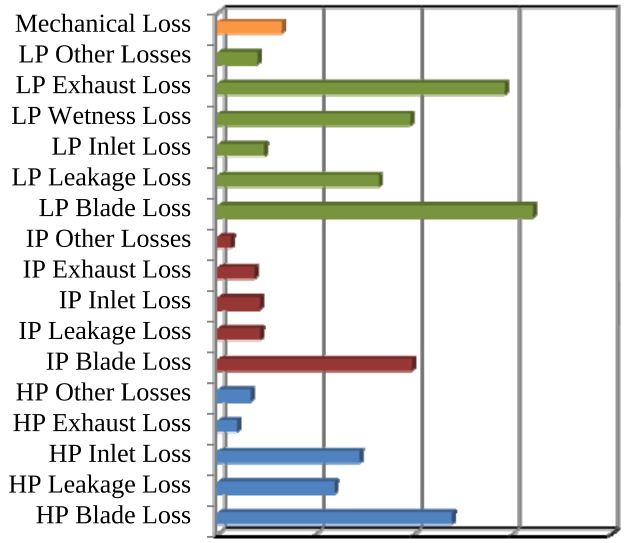

Figure 2. BREAKDOWN OF THE TYPICAL LOSSES OF A RECENT LARGE-SCALE STEAM TURBINE (RELATIVE FRACTIONS OF EACH LOSS)

NOMENCRATURE

e	Total internal energy per unit volume
I	Nucleation rate
J	Jacobian for transformation
k	Turbulent kinetic energy
n	Number density of water droplets
p	Static pressure
r	Averaged radius of droplets
r_*	Critical radius of a droplet
S_k	Source term for k equation
S_ω	Source term for ω equation
T	Static temperature
t	Physical time
W_i	Component of contravariant relative velocities
w_i	Component of relative velocities
β	Condensate mass fraction
Γ	Mass generation rate of liquid phase

σ_{kj}	Diffusion term for k equation
$\sigma_{\omega j}$	Diffusion term for ω equation
ρ	Density of water vapor
κ	Laminar thermal conductivity coefficient
κ^t	Turbulent thermal conductivity coefficient
Ω	Angular velocity of rotation
ω	Turbulent kinetic energy dissipation ratio
ξ_i	Component of general curvilinear coordinates
τ_{ij}	Viscous stress tensors

Subscripts

v	Water vapor
l	Water liquid

FUNDAMENTAL EQUATIONS

The fundamental equations in this study consist of conservation laws of total density, momentum, total energy, water vapor density, liquid water density, and the number density of water droplets. They are coupled with the shear stress transport (SST) turbulence model[24] with relative velocities in general curvilinear coordinates as

$$\frac{\partial Q}{\partial t}+\frac{\partial F_i}{\partial \xi_i}+S+H=0 \tag{1}$$

where Q, F_i (i=1,2,3), S, and H are vectors of unknown variables, the vector of flux, the viscous term, and the source term, respectively. They are defined as follows:

$$Q=J\begin{bmatrix}\rho\\ \rho w_1\\ \rho w_2\\ \rho w_3\\ e\\ \rho_v\\ \rho\beta\\ \rho n\\ \rho k\\ \rho\omega\end{bmatrix},\quad F_i=J\begin{bmatrix}\rho W_i\\ \rho w_1 W_i+\partial\xi_i/\partial x_1 p\\ \rho w_2 W_i+\partial\xi_i/\partial x_2 p\\ \rho w_3 W_i+\partial\xi_i/\partial x_3 p\\ (e+p)W_i\\ \rho_v W_i\\ \rho\beta W_i\\ \rho n W_i\\ \rho k W_i\\ \rho\omega W_i\end{bmatrix},$$

$$S=-J\frac{\partial\xi_i}{\partial x_j}\frac{\partial}{\partial\xi_i}\begin{bmatrix}0\\ \tau_{1j}\\ \tau_{2j}\\ \tau_{3j}\\ \tau_{kj}u_k+(\kappa+\kappa^t)\partial T/\partial x_j\\ 0\\ 0\\ 0\\ \sigma_{kj}\\ \sigma_{\omega j}\end{bmatrix},$$

$$H=-J\begin{bmatrix}0\\ 0\\ \rho\left(\Omega^2x_2+2\Omega w_3\right)\\ \rho\left(\Omega^2x_3-2\Omega w_2\right)\\ 0\\ -\Gamma\\ \Gamma\\ I\\ S_k\\ S_\omega\end{bmatrix}$$

In the source term, the Coriolis and centrifugal forces due to rotation are taken into account.

CONDENSATION MODEL

The equation of state and the speed of sound in wet steam were derived by Ishizaka, Ikohagi, and Daiguji[25] assuming that the condensate mass fraction β is sufficiently small (β <0.1) as

$$p=\rho RT(1-\beta) \tag{2}$$

$$c^2=\frac{C_{pm}}{C_{pm}-(1-\beta)R}\frac{p}{\rho} \tag{3}$$

where C_{pm} is defined as the linear combination of the isobaric specific heat between the gas and liquid phases using the mass fraction β.

The mass generation rate Γ for water droplets is derived as a sum of the mass generation rate of a critical-sized nucleus and the growth rate of a water droplet based on the classical condensation theory. It was further approximated by Ishizaka et al. [25] as:

$$\Gamma=\frac{4}{3}\pi\rho_l\left(Ir_*^3+3\rho nr^2\frac{dr}{dt}\right) \tag{4}$$

where the homogeneous nucleation rate I defined by Frenkel [26] and the growth rate of a water droplet dr/dt proposed by Gyarmathy [27] are employed.

NUMERICAL METHODS

The high-order high-resolution finite-difference method that is based on the fourth-order compact MUSCL TVD(Compact MUSCL) scheme[21] and Roe's approximate Riemann solver[22] is used for space discretization of the convection terms in Eq.(1). The viscosity term is calculated using the second-order central-difference scheme.

A parallel-implicit computational algorithm based on pipeline processing assisted by OpenMP was applied to the LU-SGS scheme [23] in order to reduce CPU times. The LU-SGS scheme is given as:

$$D\Delta Q^* = RHS \ + \Delta t G^+\left(\Delta Q^*\right)$$
$$\Delta Q = \Delta Q^* - D^{-1}\Delta t G^-\left(\Delta Q\right) \quad (5)$$

where *RHS* is the vector of the explicit time-marching residues of Eq.(1), Δt is the time step, *D* is the diagonal matrix approximated by the spectral radius of Jacobian matrices, and G^+ and G^- are functions composed of time derivatives of numerical flux at neighboring grid points and are defined by the equations:

$$G^+\left(\Delta Q^*\right) = \left(A_1^+\Delta Q^*\right)_{i-1,j,k} + \left(A_2^+\Delta Q^*\right)_{i,j-1,k} + \left(A_3^+\Delta Q^*\right)_{i,j,k-1}$$
$$G^-\left(\Delta Q\right) = \left(A_1^-\Delta Q\right)_{i+1,j,k} + \left(A_2^-\Delta Q\right)_{i,j+1,k} + \left(A_3^-\Delta Q\right)_{i,j,k+1}$$

The subscripts, *i*, *j*, and *k* indicate a grid point where time derivatives of numerical flux are located. CPU time has been reduced by employing the algebraic approximation of *D*. The calculations should be executed sequentially, as the calculation at a particular grid point depends on those at adjacent points during the same time-step. The computational algorithm for the LU-SGS scheme is not always suitable for parallel computation. When the wet-steam flow through a 3D single channel was calculated using a single CPU, approximately 40% of the total CPU time for each iteration was dedicated to computing the LU-SGS. With the assistance of OpenMP, pipeline processing is applied to the hyper-plane of the LU-SGS sweeps, following which the hyper-plane can then be divided into multiple blocks. The lower block is calculated using one CPU and the upper block is calculated using another CPU. The computation at the lower block commences first, and then the computation at the upper block begins, using boundary data already calculated in the lower block. Each CPU performs its calculation simultaneously according to the movement of the hyper-plane. The number of CPUs can be easily increased in the same manner and replaced with 2 CPUs. Finally utilizing either 4 or 8 CPUs was found to be most effective and economical for the pipelined LU-SGS calculation in the present code.

FINDINGS FROM SCALE MODEL TESTS

In order to improve the performance of the steam turbine exhaust hood, the effects of shapes of both casings and diffusers were studied using numerical analysis and model exhaust hood tests. These numerical analyses made it possible to predict complex three dimensional flows in exhaust hoods, and comparisons were made between calculated pressure loss results and the model test results. Figure 3 shows a low pressure exhaust hood test rig at Toshiba [2]. Figure 4 shows the oil flow visualization on the outer wall surface of the low pressure exhaust diffuser (left) and the computed limiting stream lines on the same diffuser surface [2]. These experimental and computational results show that there are some boundary layer separations on the outer wall surface near the outlet rim of the exhaust diffuser. In large-scale steam turbine designs, axial lengths of low pressure casings and rotors need to be shortened in order to minimize the clearances between rotor or rotating blades and stationary walls. Consequently, the axial lengths of the exhaust diffusers need to be at a minimum while maintaining the required performance. This makes it difficult to design perfect diffusers that do not have any boundary layer separations. However, the findings of these model exhaust diffuser tests and analyses indicate that there is scope for the further enhancement of the aerodynamic efficiency of these types of exhaust diffusers. Following these scale model tests, we conducted detailed aerodynamic measurements and very accurate numerical investigations of exhaust hoods in a full-scale low pressure turbine.

Figure 3. LP EXHAUST HOOD TEST RIG AT TOSHIBA [2]

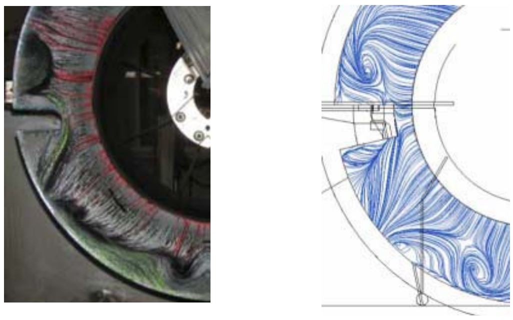

Figure 4. OIL FLOW VISUALIZATION ON THE OUTER WALL SURFACE OF THE LP EXHAUST DIFFUSER (LEFT) AND COMPUTED LIMITING STREAM LINES ON THE SAME DIFFUSER SURFACE (RIGHT) [2]

MEASUREMENTS IN A FULL SCALE DEVELOPMENT STEAM TURBINE

For final verification of the developed LP turbine and exhaust hood design, full-scale development steam turbine tests were carried out [4]. Figure 5 shows an LP rotor in lower casing (left) and LP outer casing (right) of the Toshiba Full Scale Development Steam Turbine. The exhaust diffuser for this development turbine has a geometry that is typical of current large-scale steam turbines.

Measurements of this full scale development turbine can take into account the influence of inlet turbulence and radial distribution of total pressure and velocity vectors including tip leakage induced by six turbine stages upstream from the exhaust diffuser.

Figure 5. TOSHIBA FULL SCALE DEVELOPMENT STEAM TURBINE, LP ROTOR IN LOWER CASING (LEFT) AND LP OUTER CASING (RIGHT) [4]

The total and static pressures in the inlet and outlet positions of the LP exhaust diffuser were measured in this full-scale development steam turbine. The flow angles and velocity distribution including the rotor blade tip leakage region were also measured. All measurement data are used for the following numerical investigation.

COMPARISON BETWEEN NUMERICAL AND EXPERIMENTAL RESULTS

Table 1 shows the flow conditions for measurements of the exhaust diffuser in this development turbine. The inlet Reynolds number is defined using viscosity, density, velocity and flow path height at the diffuser inlet traverse measurement section just downstream of the last stage rotating blades. The static pressures were measured in eight circumferentially equally spaced pressure taps that are located on each inner and outer diffuser walls and the measured pressures are averaged and shown in Table 1. Inlet total pressures are measured using four fixed and one traversing probes and the measure data are also circumferentially averaged.

The exhaust diffuser measurement errors obtained using the current measurement system (pressure transducers and probes) are within 0.5%.

Table 1. FLOW CONDITIONS

Flow condition parameters	Measured data
Inlet total pressure [kPa]	4.40
Outlet static pressure [kPa]	4.05
Inlet wetness (%)	3.5
Inlet Mach number	0.54
Inlet Reynolds number	530000

Figure 6(a) shows the computational domain for the LP exhaust diffuser. Since the measured circumferential distribution of total and static pressures at the outlet section of the exhaust diffuser was small and not dominant on the diffuser flow in this turbine, circumferentially averaged inlet and outlet boundary conditions are used. A quarter part of the full volume of the diffuser was calculated with circumference symmetric boundary conditions on both circumferential cutting sections. Figure 6(b) shows the meridional view of the computational grid system. In order to enhance the degree of freedom allowing local control of grid point locations, the grid system consists of two grid blocks. The total grid system consists of 182 stream-wise, 46 circumferential-wise and 97 radial-wise grid points.

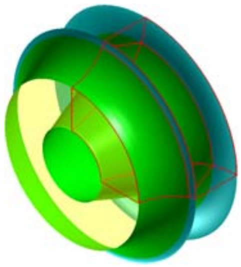

Figure 6(a). COMPUTATIONAL DOMAIN FOR THE LP EXHAUST DIFFUSER

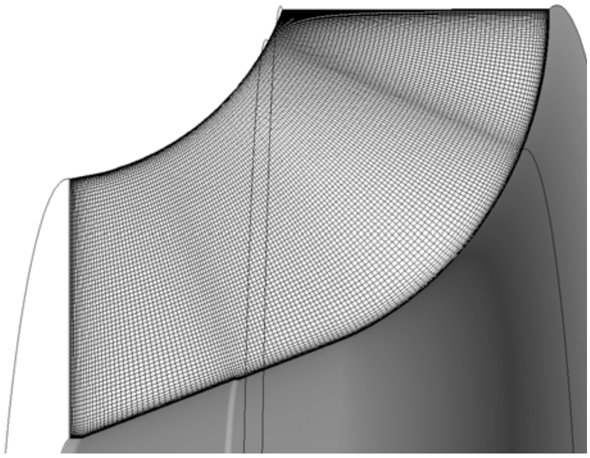

Figure 6(b). MERIDIONAL VIEW OF THE COMPUTATIONAL GRID SYSTEM

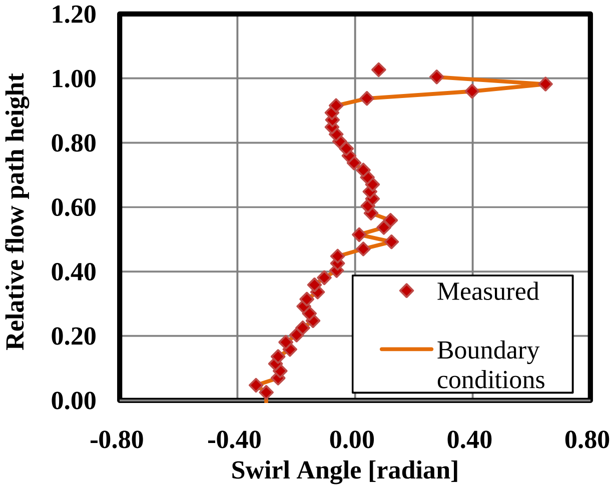

Figure 7(a). MEASURED AND BOUNDARY CONDITION SWIRL ANGLE DISTRIBUTIONS AT THE EXHAUST DIFFUSER INLET SECTION

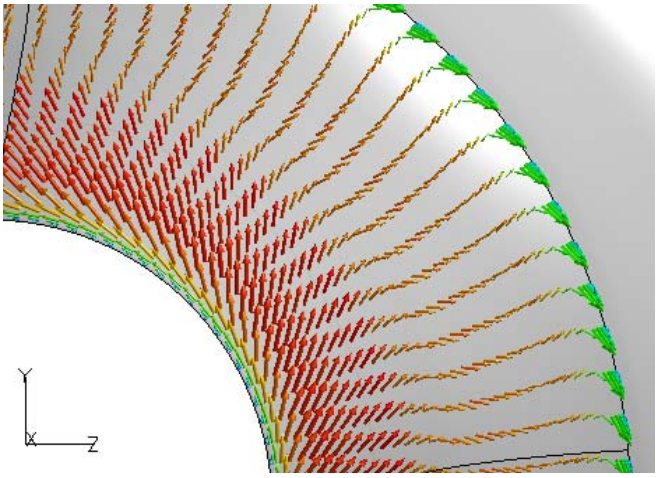

Figure 7(b). BOUNDARY CONDITION VELOCITY VECTORS AT EXHAUST DIFFUSER INLET SECTION (UPSTREAM VIEW)

Figure 7(a) shows the measured swirl angle distributions at the exhaust diffuser inlet section. It includes the tip leakage region. This measured swirl angle distribution was used as the inlet boundary condition for present numerical investigations.

Figure 7(b) shows boundary condition velocity vectors at the exhaust diffuser inlet section as viewed from upstream of the diffuser.

It is very difficult to accurately measure the turbulence intensity in the wet steam and high speed flow condition just downstream of the last stage rotating blades in a full-scale steam turbine. An alternative that we introduced is the calculated turbulence intensity just downstream of a multi stage turbine from unsteady three dimensional wet steam flow analyses for the inlet condition.

Figure 8(a) shows the calculated Mach number contours having an inlet turbulence boundary condition of the stage exit condition. Figure 8(b) shows the calculated Mach number contours having no inlet turbulence boundary condition. The boundary layer decelerating and separation region near outer downstream of the diffuser in Figure 8(b) is larger than that of Figure 8(a). Figure 9(a) shows the calculated stream lines with inlet turbulence of the stage exit condition, and Figure 9(b) shows the calculated stream lines without inlet turbulence. Figure 9(b) also shows a vortex system of stream lines that is larger than that of Figure 9(a). These figures illustrate that inlet turbulence reduces the boundary layer separation region. From the comparison study between calculated and measured results, we chose the case using inlet turbulence from stage exit condition as the more realistic inlet condition for the following numerical investigations. More quantitative discussions are presented in the later section.

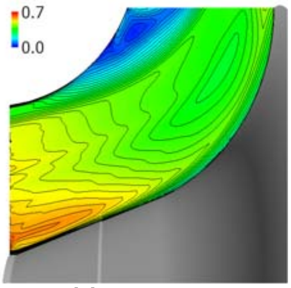

Figure 8(a). CALCULATED MACH NUMBER CONTOURS WITH INLET TURBULENCE BOUNDARY CONDITION FROM MEASUREMENTS

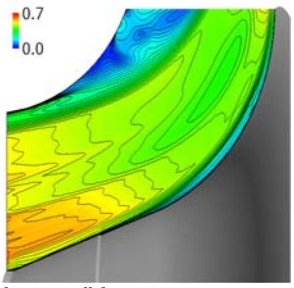

Figure 8(b). CALCULATED MACH NUMBER CONTOURS WITH NO INLET TURBULENCE BOUNDARY CONDITION

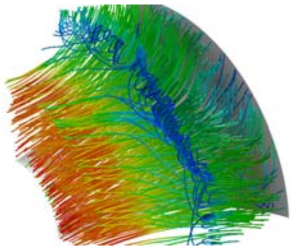

Figure 9(a). CALCULATED STREAM LINES WITH INLET TURBULENCE BOUNDARY CONDITION FROM MEASUREMENTS

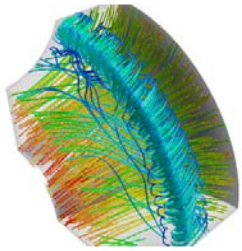

Figure 9(b). CALCULATED STREAM LINES WITH NO INLET TURBULENCE BOUNDARY CONDITION

Figures 10-14 present detailed numerical investigation results that compare calculations both with and without a steam condensation model. Figures 10(a) and 10(b) show calculated Mach number contours. The diffuser inlet flow decelerate continuously from the inlet to the outlet with a separation region existing on the outer wall near outlet. Figures 11(a) and 11(b) show the calculated static pressure contours that illustrate the static pressure recovery and static pressure decrease from the outlet to the inlet of the diffuser. Figure 12 shows the calculated wetness contours. As static enthalpy increases, the wetness decreases from the inlet to the outlet, while the velocity energy changes to the static pressure increase. Since both the static enthalpy and entropy increase in the separation region, the wetness in the separation region becomes very low. Figure 13 shows the calculated eddy viscosity contours while Figure 14 shows the calculated turbulent kinetic energy contours. It is possible to identify the region where aerodynamic losses are generated around the tip leakage and the wake of mid-span shrouds just downstream of the last stage rotating blade (at the inlet of the exhaust diffuser) and around the separation region and boundary layers on the diffuser walls.

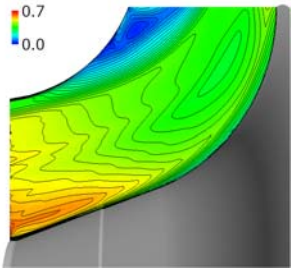

Figure 10(a). CALCULATED MACH NUMBER CONTOURS WITH CONDENSATION MODEL

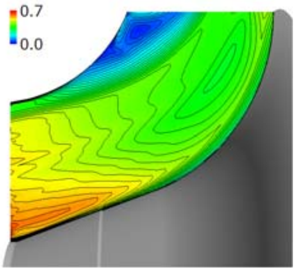

Figure 10(b). CALCULATED MACH NUMBER CONTOURS WITHOUT CONDENSATION MODEL

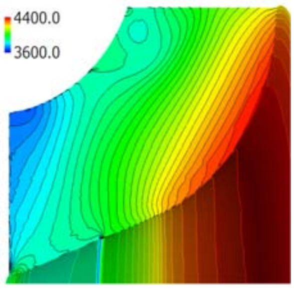

Figure 11(a). CALCULATED STATIC PRESSURE CONTOURS WITH CONDENSATION MODEL

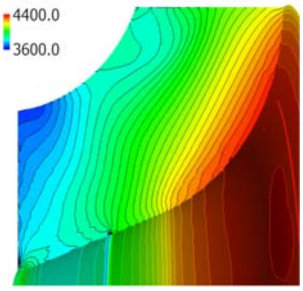

Figure 11(b). CALCULATED STATIC PRESSURE CONTOURS WITHOUT CONDENSATION MODEL

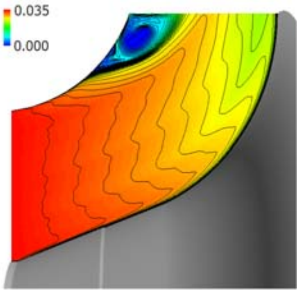

Figure 12. CALCULATED WETNESS CONTOURS WITH CONDENSATION MODEL

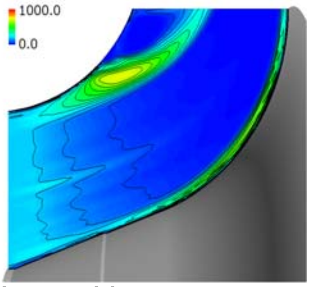

Figure 13(a). CALCULATED EDDY VISCOSITY CONTOURS WITH CONDENSATION MODEL

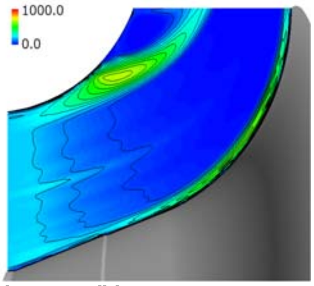

Figure 13(b). CALCULATED EDDY VISCOSITY CONTOURS WITHOUT CONDENSATION MODEL

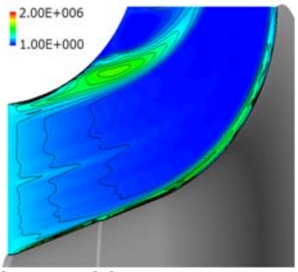

Figure 14(a). CALCULATED TURBULENT KINETIC ENERGY CONTOURS WITH CONDENSATION MODEL

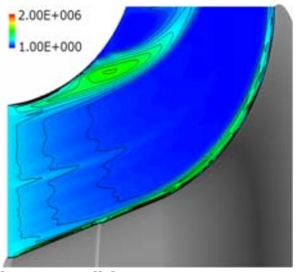

Figure 14(b). CALCULATED TURBULENT KINETIC ENERGY CONTOURS WITHOUT CONDENSATION MODEL

With the exception of the wetness contours, these figures show that the condensation model does not have a large impact on the flow field of the diffuser. This small effect is thought to be due to the low value of both the inlet wetness and the inlet Mach number (around 0.5 to 0.6).

Figure 15 shows the calculated meridional velocity vectors at the same condition as Figure 8(a) and Figure 10(a). In the boundary layer separation region that is on the wall surface near the outlet rim of the diffuser outer wall (enlarged velocity vectors are shown in the box), the reverse flow is moderate and appears to be a noncritical condition for this exhaust diffuser design. On the inner concave wall, a thick boundary layer can be seen, but there is no separation region and in this case, the aerodynamic loss generation appears to be small. Figure 16 shows the calculated limiting stream lines of the diffuser outer wall surface which seem to indicate strong swirl flows around the separation region. Figure 17 shows the calculated limiting stream lines of the diffuser inner surface on which there is no separation, and the swirl component of the boundary layer flow is small.

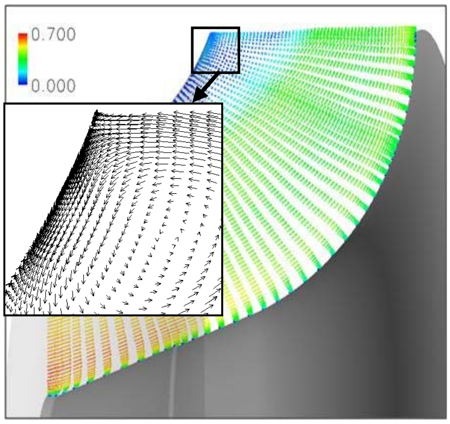

Figure 15. CALCULATED MERIDIONAL VELOCITY VECTORS

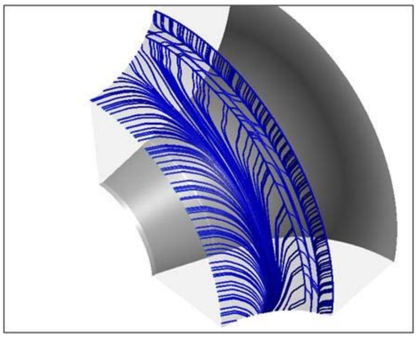

Figure 16. CALCULATED LIMITING STREAM LINES OF DIFFUSER OUTER SURFACE

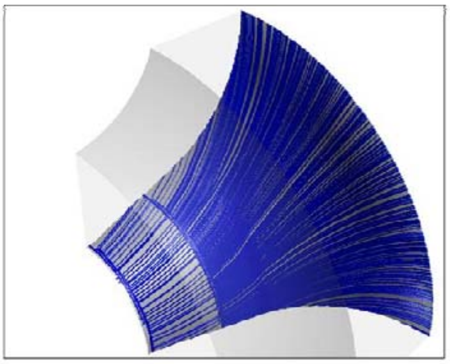

Figure 17. CALCULATED LIMITING STREAM LINES OF DIFFUSER INNER SURFACE

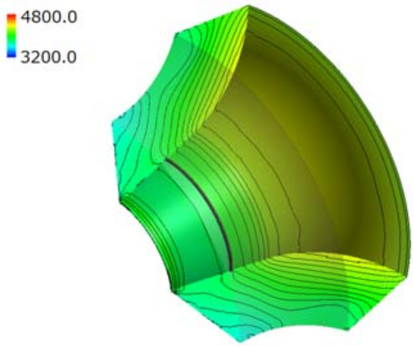

Figure 18. CALCULATED STATIC PRESSURE CONTOURS ON INNER SURFACE AND CIRCUMFERENTIAL CYCLIC CALCULATION BOUNDARY SURFACES (VERTICAL AND HORIZONTAL)

Figure 18 shows the calculated static pressure contours on the inner surface and the vertical and horizontal circumferential cyclic boundary surfaces. There is a small variation in the circumferential distribution of the static pressure contours. The unsteady flow field of the diffuser seems to generate these small static pressure fluctuations.

Figure 19 shows the comparison between the measured pressures and the results of the numerical calculations without inlet turbulence. All of the pressures in Figures 19, 20 and 21 are normalized relative to the inlet total pressure. The outlet total pressure distributions were measured at four different circumference angle positions (the 4 degree probe was located near the top, the 95 degree probe was located near the horizontal joint, the 208 degree probe was located near the bottom and the 265 degree probe was located near the horizontal joint). We can find a similar distribution in any position, but the calculated outlet total pressure distribution is different. This indicates the generation of a very large boundary layer separation near the outer wall for flow path height values ranging from 0.6 to 1.0.

Figure 20 shows the comparison between measured pressures and the results of calculations using inlet turbulence from the stage exit condition and condensation model. In this case, there is good agreement between measured and calculated results. Figure 21 shows the comparison between measured pressures and the results of calculation using inlet turbulence from the stage exit condition but without the condensation model. This case also shows good agreement between measured and calculated results.

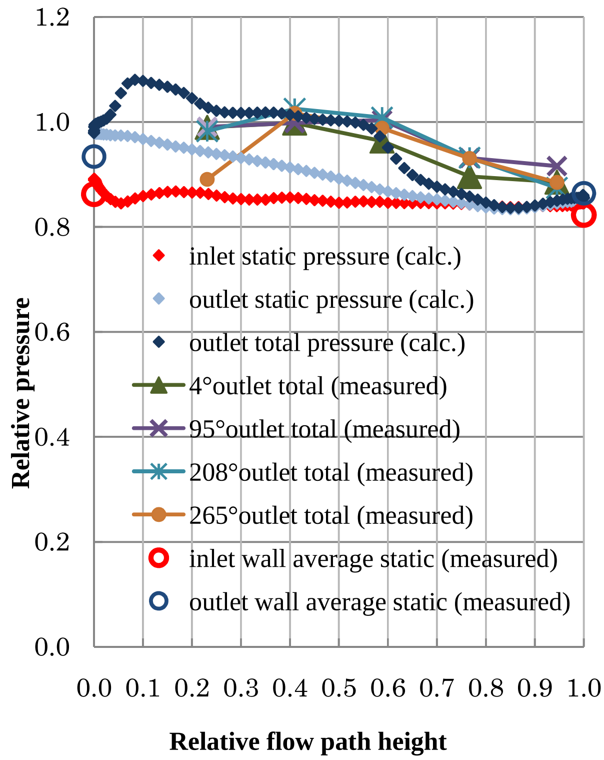

Figure 19. COMPARISON BETWEEN MEASURED AND CALCULATED PRESSURES WITH NO INLET TURBULENCE BOUNDARY CONDITION

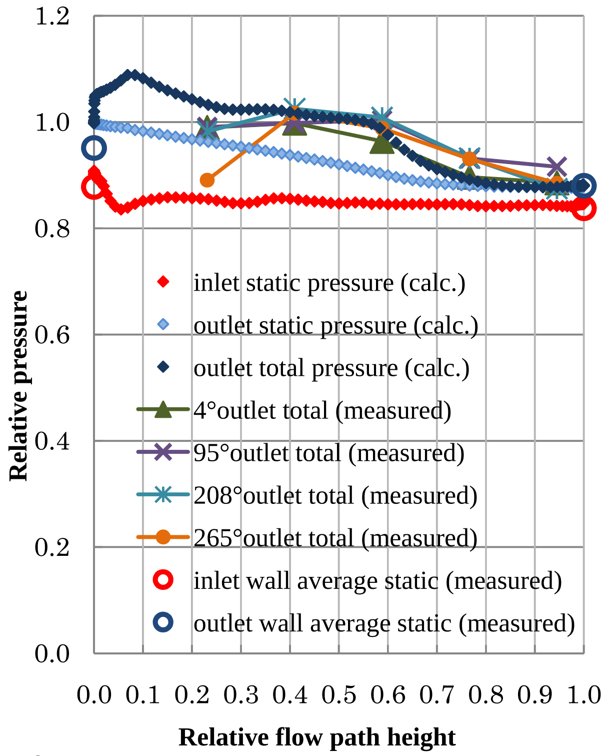

Figure 20. COMPARISON BETWEEN MEASURED AND CALCULATED PRESSURES WITH CONDENSATION MODEL

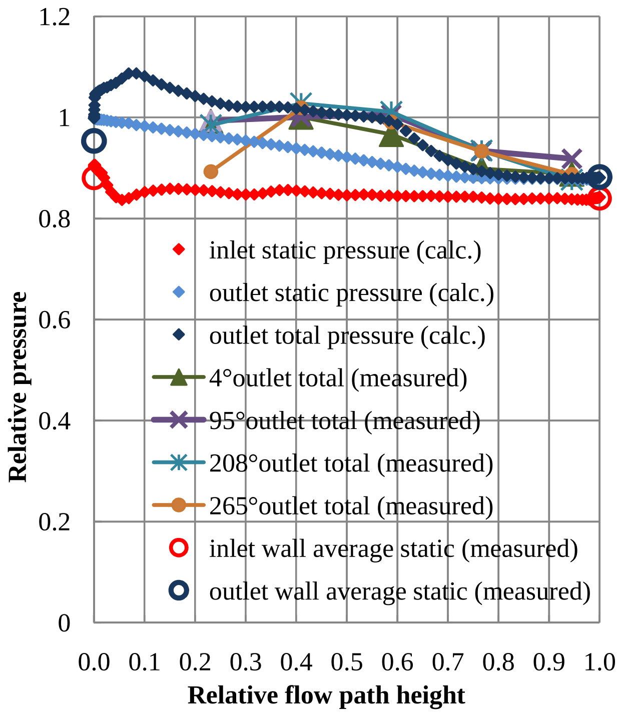

Figure 21. COMPARISON BETWEEN MEASURED AND CALCULATED PRESSURES WITHOUT CONDENSATION MODEL

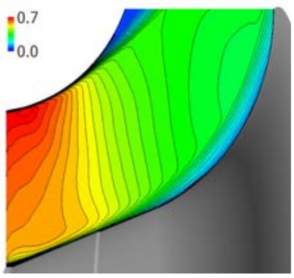

Figure 22(a). CALCULATED MACH NUMBER CONTOURS WITH ARTIFICIAL FLAT INLET FLOW DISTRIBUTION CONDITION

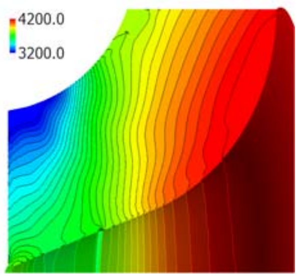

Figure 22(b). CALCULATED STATIC PRESSURE CONTOURS WITH ARTIFICIAL FLAT INLET FLOW DISTRIBUTION CONDITION

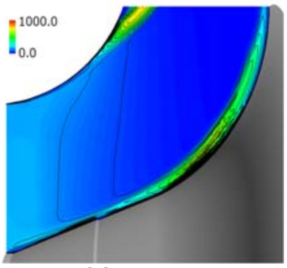

Figure 23(a). CALCULATED EDDY VISCOSITY CONTOURS WITH ARTIFICIAL FLAT INLET FLOW DISTRIBUTION CONDITION

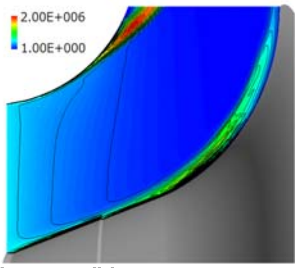

Figure 23(b). CALCULATED TURBULENT KINETIC ENERGY CONTOURS WITH ARTIFICIAL FLAT INLET FLOW DISTRIBUTION CONDITION

In order to evaluate the influence of the distribution of the inlet boundary condition, using a uniform inlet flow condition that has a simple wall boundary layer velocity deficit model on both inner and outer diffuser walls, the uniform inlet case having an artificial flat inlet flow distribution condition was calculated.

Figure 22(a) shows calculated Mach number contours and Figure 22(b) shows calculated static pressure contours. Figure 23(a) shows calculated eddy viscosity contours and Figure 23(b) shows calculated turbulent kinetic energy contours. If the inlet boundary condition had been uniform, the boundary layer separation would have been very small and the diffuser aerodynamic efficiency would increase. However, this case is not realistic and this result emphasizes the need to exercise caution in ensuring that turbine diffuser efficiency is not overestimated by this kind of independent analysis. However, we can extract some useful findings from these numerical studies that will allow us to increase the diffuser efficiency.

CONCLUSIONS

An accurate unsteady numerical analysis is introduced for the simulation of diffuser flows in LP exhaust hoods. Compressible Navier-Stokes equations are solved using the high-order high-resolution finite-difference method including the wet steam condensation model. The inlet conditions were introduced from full scale steam turbine tests and calculation results are compared with measured data of the same full scale steam tests.

Pressure, velocity and flow angle distributions of inlet boundary conditions are critical parameters to consider when carrying out numerical investigations of steam turbine LP exhaust diffusers. These parameters should include the influence of upstream turbine stages.

Inlet turbulence intensity just downstream of the upstream turbine stages is also necessary for numerical analyses of turbine diffusers.

The flow fields of current LP exhaust diffusers having a geometry that is typical of large-scale steam turbines can be accurately calculated if we use the correct inlet boundary conditions from the flow distribution just downstream of the last stage turbine blades.

Using the calculated turbulence intensity just downstream of the last stage turbine blade increases the accuracy of the numerical calculation around the separation region.

Numerical calculations using flat inlet flow distribution in the present exhaust diffuser resulted in a good and efficient flow field having a very small separation region. However, the diffuser efficiency may be overestimated.

The present numerical method was validated with the measurement data of the LP exhaust diffuser in the full-scale development steam turbine, and this method is acceptable in the development of optimum designs for which revised geometries are introduced in an effort to enhance steam turbine efficiency.

ACKNOWLEDGMENT

The present computations were performed using the Earth Simulator Center of Japan Agency for Marine-Earth Science and Technology. The authors wish to acknowledge the support from the Earth Simulator Center.

REFERENCES

[1] DOE/EIA, 2010. International Energy Outlook 2010, pp. 77-95.

[2] Iwai, Y., Saeki, H., Niizeki, Y., Ohishi, T., Tanuma, T. and Sasaki, T., 2009. “Development of High Performance Low Pressure Exhaust Hoods for Steam Turbine”. Conference Paper of JSME Power and Energy Engineering Division, pp. 100-103 (in Japanese).

[3] Tanuma, T., Sasaki, T. and Niizeki, Y., 2007. “Performance Enhancement of Large-Scale Steam Turbines Using CFD”. Toshiba Review, Vol.62, No.9, pp.25-29 (in Japanese).

[4] Shibukawa, N., Kawasaki, S., Kawakami, H., Okuno, K., Niizeki, Y., Suzuki, T. and Sasaki, T., 2009. “The Actual Size Steam Turbine Development Facility Mikawa Power Station Unit-2”. Proceedings of the International Conference on Power Engineering-09, Kobe, Japan.

[5] Sovran, G., and Klomp, E. D., 1965. “Experimentally Determined Optimum Geometries for Rectilinear Diffusers with Rectangular, Conical or Annular Cross-Section”. General Motors Corporation Research Publication, GMR-511.

[6] Xu, S., Kang, S. and CH. Hirsch, 2001. “Numerical Simulation of the 3D Viscouse Flow in the Exhaust Casing of a Low-Pressure Steam Turbine”. ASME paper No. 2001-GT-0487.

[7] Liu, J., Cui, Y. and Jiang, H., 2001. “Investigation of Flow in a Steam Turbine Hood with/without Turbine Exit Conditions Simulated”. ASME paper No. 2001-GT-0488.

[8] Liu, J. J. and Hynes, T. P., 2002. “The Investigation of Turbine and Exhaust Interactions in Asymmetric Flows Part 1 Blade-Row Models Applied”. ASME paper No. 2002-GT-30342.

[9] Liu, J. J. and Hynes, T. P., 2002. “The Investigation of Turbine and Exhaust Interactions in Asymmetric Flows Part 2 Turbine-Diffuser-Collector Interactions”. ASME paper No. 2002-GT-30343.
[10] Vassiliev, V., Irmisch, S. and Florjancic, S., 2002. “CFD Analysis of Industrial Gas Turbine Exhaust Diffusers”. ASME paper No. 2002-GT-30597.
[11] Fu, J. L., Zhou, S. J. and Liu, J. J., 2008. “Experimental and Numerical Investigation of Interactions between Axial Turbine and Non-axisymmetric Exhaust Hood”. ASME paper No. GT2008-50766.
[12] Sanz, W., Kelterer, M., Pecnik, R., Marn, A. and Gottlich, E., 2009. “Numerical Investigation of the Effect of Tip Leakage Flow on an Aggressive S-Shaped Intermediate Turbine Duct”. ASME paper No. GT2009-59535.
[13] Fu, J. L. and Liu, J. J., 2010. “Investigations of Influential Factors on the Aerodynamic Performance of a Steam Turbine Exhaust System”. ASME paper No. GT2010-22316.
[14] Yamamoto, S. and Tanuma, T., 1999. “Numerical Study of Unsteady Gas and Steam Turbine Cascade Flows”. Proceedings of the International Gas Turbine Congress, pp. 489-496.
[15] Yamamoto, S., Sasao, Y., Sato, S., and Sano, K., 2007. “Parallel-Implicit Computation of Three-dimensional Multistage Stator-Rotor Cascade Flows with Condensation”. Proc. 18th AIAA Computational Fluid Dynamics Conference, AIAA Paper 2007-4460.
[16] Yamamoto, S., Sasao, Y., Sano, K., Satsuki H., Ishizaka, K., and Ooyama, H., 2007. “Parallel Computation of Condensate Flows through 2-D and 3-D Multistage Turbine Cascades”. Proc. International Gas Turbine Congress 2007, Tokyo, CD-ROM.
[17] Yamamoto, S., Hagari, H. and Murayama, M., 2000. “Numerical Simulation of Condensation around the 3-D Wing”. Trans. of the Japan Society of Aeronautical and Space Sciences, 42-138, pp. 182-189.
[18] Yamamoto, S., 2003. “Onset of Condensation in Vortical Flow over Sharp-edged Delta Wing”. AIAA Journal, 41-9, pp. 1832-1835.
[19] Yamamoto, S., 2005. “Computation of Practical Flow Problems with Release of Latent Heat”. ENERGY, 30, pp. 197-208.
[20] Sasao, Y. and Yamamoto, S., 2005. “Numerical Prediction of Unsteady Flows through Turbine Stator-rotor Channels with Condensation”. Proc. ASME Fluids Engineering Summer Conference, FEDSM2005- 77205, CD-ROM.
[21] Yamamoto, S. and Daiguji H., 1993. “Higher-Order-Accurate Upwind Schemes for Solving the Compressible Euler and Navier-Stokes Equations”. Computers and Fluids, 22-2/3, pp. 259-270.
[22] Roe, P.L., 1981. “Approximate Riemann Solvers, Parameter Vectors, and Difference Schemes”. J. Comp. Phys., 43, pp. 357-372.
[23] Yoon, S. and Jameson, A., 1988. “Lower-upper Symmetric-Gauss-Seidel method for the Euler and Navier-Stokes equations”. AIAA Journal, **26**, pp. 1025-1026.
[24] Menter, F.R., 1994. “Two-equation Eddy-viscosity Turbulence Models for Engineering Applications”. AIAA Journal, 32-8, pp. 1598-1605.
[25] Ishizaka, K., Ikohagi, T. and Daiguji, H., 1995. “A High-Resolution Finite Difference Scheme for Supersonic Wet-Steam Flows”. Proc. 6th Int. Symp. on Computational Fluid Dynamics, 1, pp. 479-484.
[26] Frenkel, J., 1955. Kinetic Theory of Liquids. Dover.
[27] Gyarmathy, G. Z., 1963. *Angew Math. Phys.*, 14-3, 280.

